Deep-Sea Research Part I 130 (2017) 30–35

Contents lists available at ScienceDirect

Deep-Sea Research Part I

journal homepage: www.elsevier.com/locate/dsri

# Opposite responses of the diurnal amplitude of sea surface temperature to the Madden-Julian Oscillation

Yunwei Yan[a,*], Zheng Ling[b], Changlin Chen[c]

[a] State Key Laboratory of Satellite Ocean Environment Dynamics, Second Institute of Oceanography, State Oceanic Administration, Hangzhou, China
[b] Guangdong Key Laboratory of Coastal Ocean Variability and Disaster Prediction, Guangdong Ocean University, Zhanjiang, China
[c] Institute of Atmospheric Sciences, Department of Environmental Science and Engineering, Fudan University, Shanghai, China

ARTICLE INFO

*Keywords:*
Opposite responses
Diurnal amplitude of sea surface temperature
Madden-Julian Oscillation
Opposing wind speed anomalies

ABSTRACT

Both observations and empirical model results show that the responses of the diurnal amplitude of sea surface temperature (DSST) to the Madden-Julian Oscillation (MJO) in the tropical regions are opposite on the two sides of a pivot longitude, which varies seasonally. This pivot longitude occurs at 180° in boreal winter, but moves to 150°E in boreal summer. When the active convection center of the MJO is located to the west of the pivot longitude, reduced solar insolation and enhanced wind speed decrease DSST; when the active convection center moves to the east of the pivot longitude, reduced wind speed increases DSST. Due to the opposing wind speed anomalies across the pivot longitude, opposite responses to the MJO can be seen in latent heat flux anomalies, evaporation rate anomalies and surface roughness anomalies. These findings suggest that opposite responses in the tropical regions on the west and east of the pivot longitude to the MJO be common for variables that are closely related to wind speed.

## 1. Introduction

As one of the fundamental periodic variations of sea surface temperature (SST), the diurnal cycle of SST has a significant influence on the ocean and atmosphere (Kawai and Wada, 2007; Guemas et al., 2013). In general, the diurnal amplitude of SST (DSST) is O(0.1 K) (Stuart-Menteth et al., 2003; Kennedy et al., 2007), but it depends primarily on solar insolation and surface wind speed, and can reach 5-7 K on a clear, calm day (Gentemann et al., 2008). Larger DSST is caused by either stronger solar radiation, which causes larger insolation absorbed at the sea surface, or lower wind speed, which causes weaker turbulent mixing in the upper ocean and less heat loss to the atmosphere (Kawai and Wada, 2007).

The Madden-Julian Oscillation (MJO), which is characterized by the eastward propagation of planetary-scale atmosphere circulation in the tropical regions coupled with deep convection over the tropical Indian and western central Pacific oceans, dominates the intraseasonal variation (30–90 days) in the tropics (Madden and Julian, 1971, 1972; Zhang, 2005). The seasonality of the MJO is featured by a latitudinal migration across the equator between the primary peak season in boreal winter (December-March) and the secondary one in boreal summer (June-September) (Zhang and Dong, 2004; Zhang, 2005). The MJO affects the degree of tropical cloudiness and hence solar radiation, zonal wind field and the ocean beneath it (Madden and Julian, 2005).

Both observations and model results demonstrate that the MJO has a large impact on DSST in the tropical Indian and western Pacific oceans (Bernie et al., 2005; Kawai and Kawamura, 2005; Bellenger and Duvel, 2009; Mujumdar et al., 2011; Li et al., 2013). Using moored observations in the western Pacific Ocean (156°E, 1°45′S) from December 1992 to March 1993, Bernie et al. (2005) found that DSST was relatively small (large) when the active (suppressed) convection center of the MJO was located in this region. This behavior was also observed in the tropical Indian Ocean (Mujumdar et al., 2011). Bernie et al. (2005) and Mujumdar et al. (2011) suggested that the MJO decreases (increases) DSST by reducing (increasing) solar insolation and enhancing (reducing) surface wind speed.

In contrast to the tropical Indian and western Pacific oceans, surface wind speed anomalies over the central tropical Pacific Ocean are negative (positive) when the active (suppressed) convection center of the MJO moves to the region (e.g., Hendon and Glick, 1997; Woolnough et al., 2000; Jin et al., 2013). This is because the climatological winds change from westerly to easterly near 180° (145°E) in boreal winter (summer) (Fig. 1). To our best knowledge, the response of DSST to the reversed wind speed anomalies associated with the MJO in the central tropical Pacific Ocean has not been reported previously. In this study, we examine the responses of DSST to the MJO over the entire tropical

* Correspondence to: Second Institute of Oceanography, State Oceanic Administration, Hangzhou 310012, China.
*E-mail address:* yanyunwei@sio.org.cn (Y. Yan).

https://doi.org/10.1016/j.dsr.2017.08.010
Received 8 October 2016; Received in revised form 20 August 2017; Accepted 21 August 2017
Available online 24 August 2017
0967-0637/ 

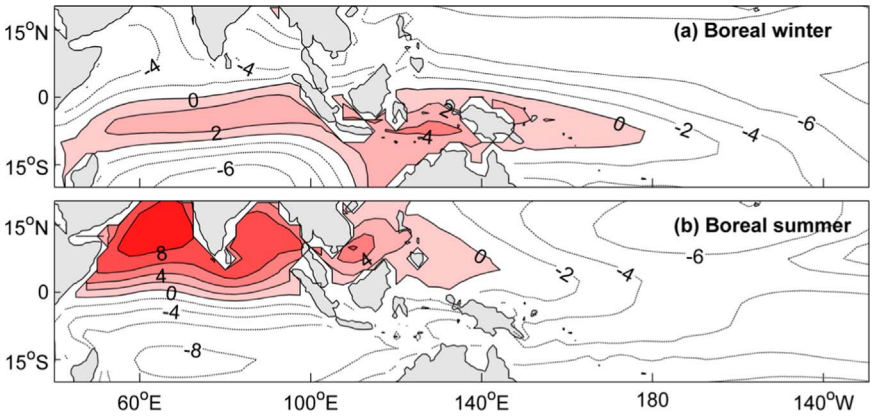


**Fig. 1.** Mean zonal wind (m/s) at 10 m in (a) boreal winter (December-March) and (b) boreal summer (June-September) during the period 1979–2013 derived from the ERA-Interim dataset.

**Table 1**
Comparison of intraseasonal signals of DSST in 2002–2003 estimated from the empirical model with the TAO/TRITON buoy data.

| | | 137°E | 147°E | 156°E | 165°E | 180° | 170°W | 155°W | 140°W |
|---|---|---|---|---|---|---|---|---|---|
| STD (Buoy) | 5°N | 0.128 | 0.147 | 0.101 | 0.134 | 0.115 | 0.127 | 0.083 | 0.063 |
| | 5°S | | | | 0.132 | 0.151 | 0.101 | 0.108 | 0.074 |
| STD (Model) | 5°N | 0.124 | 0.120 | 0.106 | 0.112 | 0.114 | 0.102 | 0.092 | 0.066 |
| | 5°S | | | | 0.138 | 0.145 | 0.096 | 0.092 | 0.077 |
| RMSE | 5°N | 0.051 | 0.052 | 0.060 | 0.052 | 0.053 | 0.050 | 0.050 | 0.039 |
| | 5°S | | | | 0.070 | 0.068 | 0.065 | 0.046 | 0.026 |
| Corr. | 5°N | 0.92 | 0.94 | 0.83 | 0.92 | 0.89 | 0.93 | 0.84 | 0.82 |
| Coef. | 5°S | | | | 0.87 | 0.89 | 0.78 | 0.91 | 0.94 |

Indian and western central Pacific oceans, especially the response of DSST to the reversed wind speed anomalies in the central tropical Pacific Ocean. We use both the Tropical Atmosphere-Ocean/Triangle Trans-Ocean Buoy Network (TAO/TRITON) data and an empirical model.

## 2. Data and method

In this study, DSST at 1 m depth is estimated from the empirical model developed by Kawai and Kawamura (2003):

$$dSST = a(MS - H_l + e)^2 + b[\ln(U)] + c(MS - H_l + e)^2[\ln(U)] + d \quad (1)$$

where $MS$, $H_l$ and $U$ are, respectively, the daily mean solar insolation (positive downward, W/m$^2$), latent heat flux (positive upward, W/m$^2$) and 10 m wind speed (m/s); $a$, $b$, $c$, and $d$ are regression coefficients; and $e$ is 300 W/m$^2$ to prevent $MS - H_l + e$ from being negative. In this estimation of DSST, the daily mean wind speed below 0.5 m/s is set to 0.5 m/s, and the estimated DSST is set to zero when it becomes negative. Kawai and Kawamura (2003) validated the model-estimated DSST with both drifting and fixed TAO buoys in the tropics within 14°S–14°N, and concluded that the model estimate of DSST has a bias of less than 0.1K and a root mean square error (RMSE) of about 0.2 K. Compared to the empirical models of Webster et al. (1996) and Kawai and Kawamura (2002), latent heat flux is introduced into this model to reduce DSST bias in the tropics (Kawai and Kawamura, 2003, 2005). The daily mean solar insolation, latent heat flux and wind speed inputs to the model are derived from the ERA-Interim global atmospheric reanalysis with a horizontal resolution of 2.5°×2.5° over the period 1979–2013 (Dee et al., 2011).

To investigate the response of DSST to the MJO in the tropical Indian and western central Pacific oceans, the Real-time Multivariate MJO (RMM) index is used to identify the strength and phase of the MJO (Wheeler and Hendon, 2004). The (RMM1, RMM2) phase space consists of eight phases. Phases 1–3, 4–5 and 6–8 indicate the enhanced convection of the MJO over the Africa and the Indian Ocean, the Maritime Continent and the Pacific Ocean, respectively. In this study, composites of DSST anomalies with $\sqrt{RMM1^2 + RMM2^2} > 1$ for each MJO phase are constructed during both boreal winter and summer. The anomaly field is calculated by subtracting the time mean and the first three harmonics of the annual cycle for the 1979–2013 period.

To further verify the response of DSST to the MJO, the TAO/TRITON buoy observations, including hourly mean SST and wind speed, along 5°S and 5°N in 2002–2003 (strong MJO activity evidenced by large $\sqrt{RMM1^2 + RMM2^2}$) are selected for analysis. DSST is estimated as the difference between the maximum temperature during the diurnal cycle and the minimum temperature in the morning. The TAO/TRITON buoy data are also used to re-evaluate the empirical model. A comparison of intraseasonal signals of DSST in 2002–2003 estimated from the empirical model with the TAO/TRITON buoy data is listed in Table 1. We can find that the differences of the standard deviation (STD) of the intraseasonal signals are less than 0.03 K with RMSEs less than 0.07 K and their correlation coefficients greater than 0.78, which illustrates that the empirical model is capable of reproducing the intraseasonal signals of DSST.

## 3. Results

Fig. 2a shows the STD of DSST intraseasonal variability in the tropical Indian and western central Pacific oceans. Generally speaking, the STD of the intraseasonal DSST is relatively large in the Indo-Pacific warm pool (greater than 0.1 K), with its maximum values located in the eastern equatorial Indian Ocean, off the coast of northwestern Australia and in the southeastern South China Sea. The variance contribution rate of the intraseasonal DSST is mostly greater than 15% in the Indo-Pacific warm pool. The intraseasonal DSST signal exhibits obvious differences in its spatial pattern between boreal winter and summer, which are characterized by a northward shift across the equator. In boreal winter, the large STD in the intraseasonal DSST is mainly confined to the Southern Hemisphere, and its maximum values appear in the Timor and Arafura Seas off the coast of northwestern Australia (Fig. 2b), while in boreal summer the large STD shifts to the Northern Hemisphere with its maximum value located in the southeastern South China Sea (Fig. 2c). Further, a comparison of the intraseasonal signals between boreal

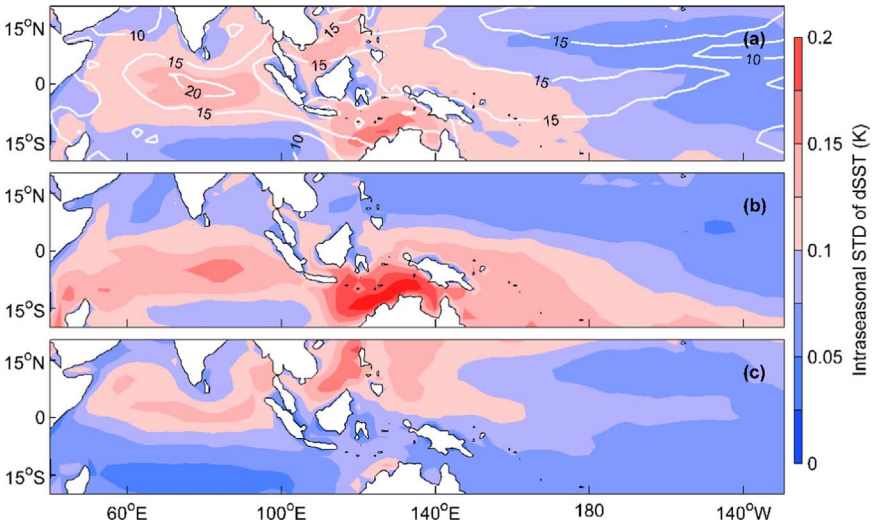


**Fig. 2.** (a) Standard deviation of the filtered (30–90 day Butterworth filter) DSST (K) in the tropical Indian and western central Pacific oceans during the period 1979–2013. (b) Same as (a) except for filtered DSST in boreal winter. (c) Same as (a) except for filtered DSST in boreal summer. Contours in (a) are variance contribution rate of the filtered DSST (%).

winter and summer shows that the DSST signal is stronger in winter than in summer.

To investigate the response of DSST to the MJO, composites of DSST anomalies for each MJO phase were constructed and are presented in Fig. 3. In boreal winter, DSST anomalies clearly show eastward propagation: Negative anomalies are located in the Indian Ocean in phases 2–3, move eastward into the Maritime Continent during phase 4, and reach their maximum intensity off the coast of northwestern Australia (-0.25 K) in phase 5. Subsequently, these negative DSST anomalies, which are confined primarily to the Southern Hemisphere, continue to propagate eastward into the tropical Pacific Ocean until they reach roughly 160°W by phases 7, 8 and 1. In the meantime, positive DSST anomalies cover the region east of 160°W. In boreal summer, negative DSST anomalies, which are located in the equatorial Indian Ocean in phase 2, move northward and extend eastward into the Pacific Ocean during phases 3–4. This motion and extension allow the maximum DSST anomalies to appear in the southeastern South China Sea (-0.2 K) by phases 5–6. In phase 7, the negative anomalies extend to about

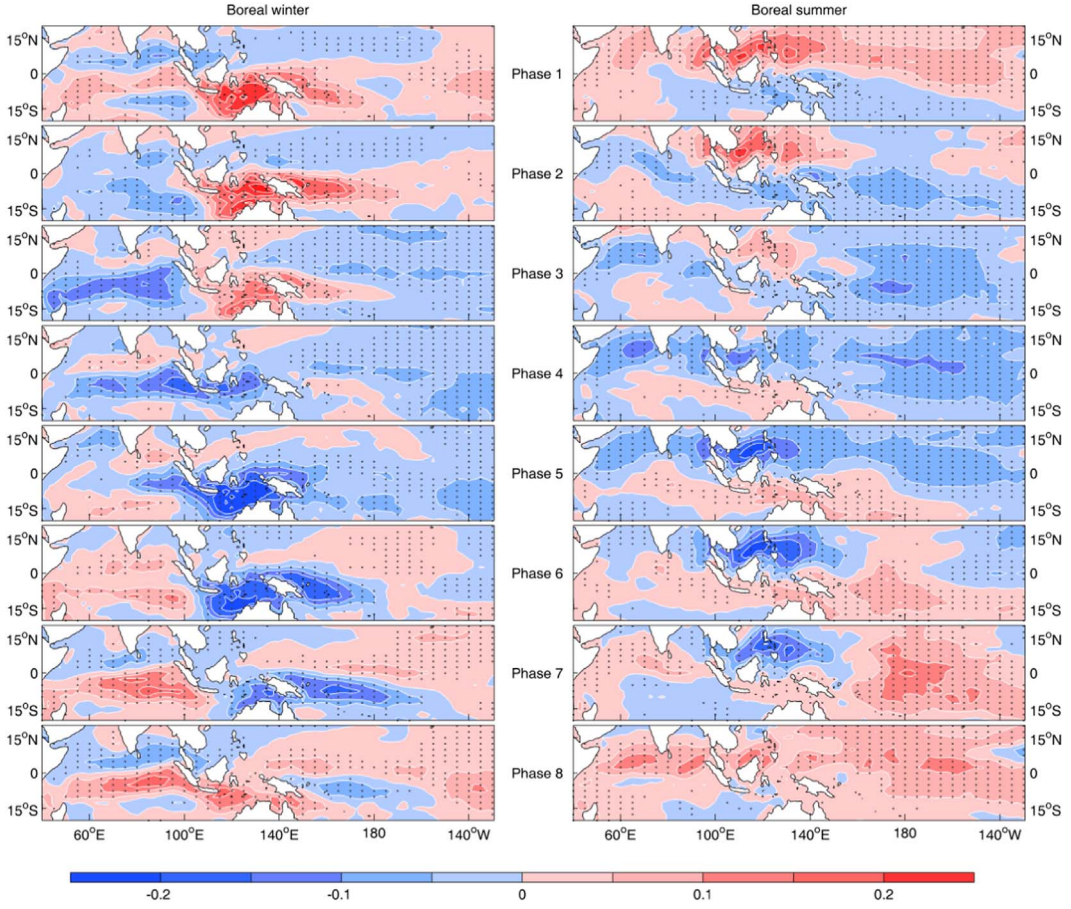


**Fig. 3.** Composites of DSST anomalies (K) for each MJO phase during boreal winter (left panels) and summer (right panels). Gray dots indicate the DSST anomalies that are statistically significant at the 99% level (Student's *t*-test).

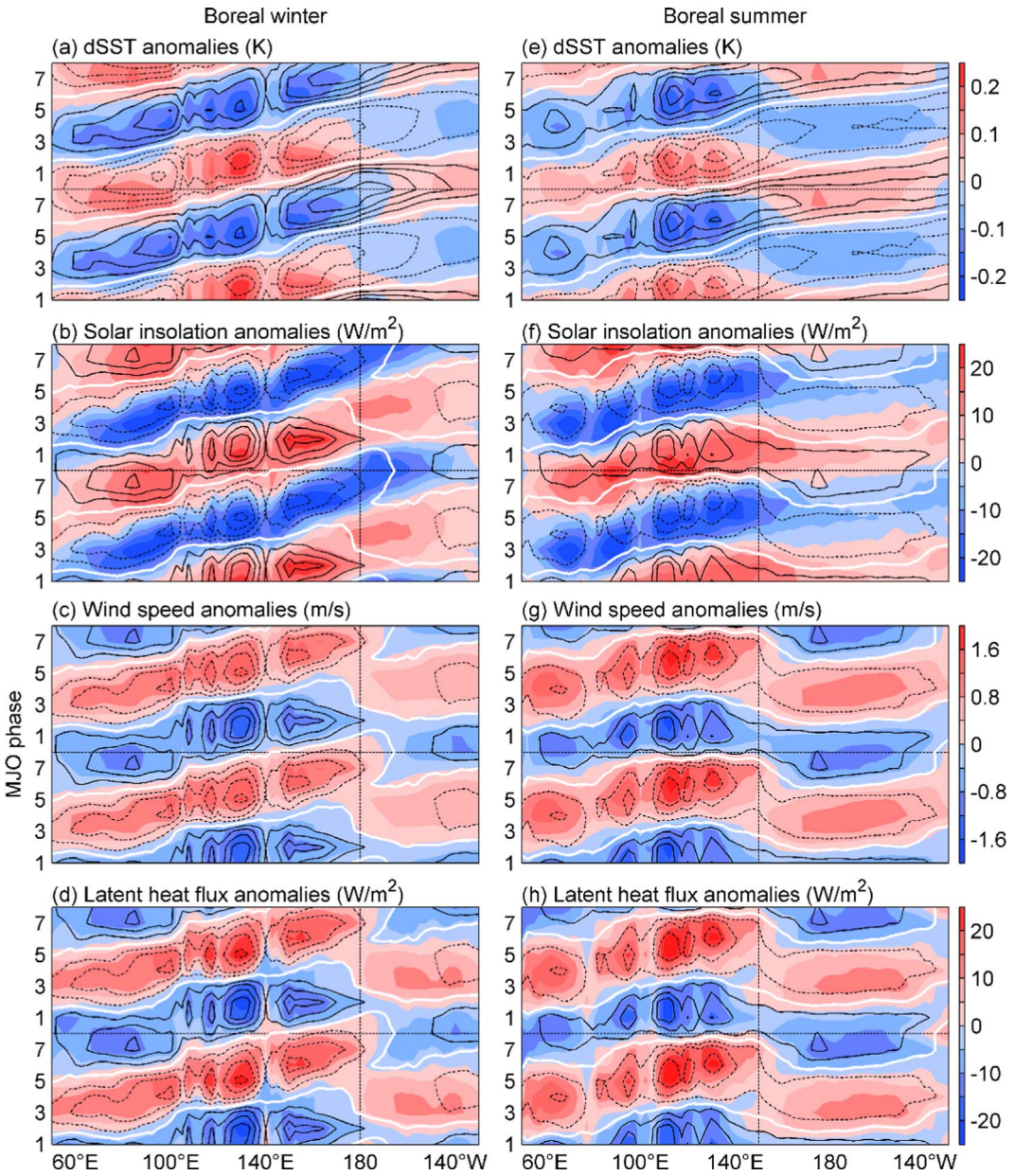


**Fig. 4.** Hovmüller diagrams for anomalies of (a, e) DSST (K), (b, f) solar insolation (W/m$^2$), (c, g) wind speed (m/s), and (d, h) latent heat flux (W/m$^2$) during boreal winter (8–2°S; left panels) and boreal summer (3–13°N; right panels). Contours are westerly/easterly anomalies in (a, e), and are DSST anomalies in the rest. Contour intervals are 0.6 m/s in (a, e) and 0.05 K in the rest. White contour denotes zero, and solid (dashed) black contours denote positive (negative) values. Vertical black line is at 180° in the left panels, and is at 150°E in the right panels. Westerly/easterly anomalies in (a, e) show the eastward propagation of the MJO.

150°E in the Northern Hemisphere, while positive DSST anomalies appear in the region east of 150°E. These positive anomalies propagate eastward during phases 8, 1 and 2.

To better reveal the propagating nature of DSST anomalies associated with the MJO, Hovmüller diagrams of DSST anomalies are shown in Figs. 4a and e. During boreal winter, negative (positive) DSST anomalies appear in the Indian Ocean during phase 2 (phase 6), and gradually move to the east until the negative (positive) anomalies become positive (negative) anomalies near 180° in phases 7, 8 and 1 (in phases 2–4). Subsequently, the positive (negative) anomalies propagate further east at much larger speeds. This propagation behavior demonstrates that the responses of DSST to the MJO during boreal winter are opposite for the tropical regions on the two sides of 180°: DSST decreases (increases) when the active (suppressed) convection center of the MJO is located to the west of 180°, consistent with the observations in Bernie et al. (2005) and Mujumdar et al. (2011), while the situation is reversed in the region east of 180°, although the DSST anomalies are relatively small in this region.

To investigate the causes of the opposite behaviors of MJO-induced changes in DSST for the regions on the two sides of 180°, Hovmüller diagrams of the anomalies of solar insolation, wind speed and latent heat flux superposed upon the DSST anomalies during boreal winter are shown in Figs. 4b-d. These diagrams show that the DSST anomalies west of 180° are determined by the combined effects of these three factors: reduced (increased) solar insolation, enhanced (reduced) wind speed and enhanced (reduced) latent heat flux decrease (increase) DSST when the active (suppressed) convection center of the MJO is located to the west of 180°, consistent with the explanation in Bernie et al. (2005) and Mujumdar et al. (2011). In the tropical Indian Ocean, the contributions of solar radiation, wind speed and latent heat flux to the variance are 40%, 38% and 12%, respectively (Yang et al., 2015). To the east of 180°, the reversed DSST anomalies are induced by reversed,

but relatively weak, wind speed and latent heat flux anomalies, while the (non-reversed) solar insolation anomalies have an opposing effect. This combination results in the relatively small DSST anomalies in this region. Because intraseasonal latent heat flux anomalies are primarily wind-driven (Araligidad and Maloney, 2008; Grodsky et al., 2009), the reversed wind speed anomalies east of 180° are the fundamental cause of the reversed DSST anomalies in this region.

Note that the MJO signals in wind speed propagate fast as free waves over the region east of 180° (Fig. 4c) (Milliff and Madden, 1996; Matthews, 2000; Zhang, 2005; Sobel and Kim, 2012), inducing fast eastward propagation of DSST anomaly signal in this region (Fig. 4a). Moreover, the anomalous winds associated with the MJO and the background winds are of the same sign when the MJO active convection center is located to the west of 180°, but are of opposite signs when the MJO suppressed phase is located over the region. This causes positive wind speed anomalies that propagate further east relative to the negative wind speed anomalies (Fig. 4c), and results in the boundary between the positive and negative DSST anomalies being located further east (Fig. 4a).

Similar to boreal winter, opposite responses of DSST to the MJO can also be seen during boreal summer, although the boundary between positive and negative DSST anomalies is shifted westward to about 150°E (Fig. 4e). The reversed DSST anomalies to the east of 150°E are induced by the reversed wind speed anomalies in this region (Figs. 4f–h). In contrast to boreal winter, the background winds in the Indian Ocean, upon which the anomalies are superimposed, are stronger during boreal summer (Fig. 1). Because DSST decreases exponentially with increasing wind speed (Gentemann et al., 2003), identical wind speed anomalies, when combined with higher background wind speed, cause smaller DSST anomalies. Thus, the DSST anomalies in the Indian Ocean are smaller during boreal summer (Figs. 4a and e).

Analysis results of the TAO/TRITON buoy data in 2002–2003 confirm the opposite responses of DSST to the MJO. To obtain MJO-induced anomalies, the maximum amplitude of the lagged regression of DSST on the RMM index is calculated. Because the maximum correlation between RMM1 and RMM2 is 0.56 at a lag of 9 days (Wheeler and Hendon, 2004), the regression results on RMM1 and RMM2 are similar. To avoid repetition, we only show the regression result for RMM2 here (Fig. 5). These results suggest that the responses of DSST to the MJO were opposite on the two sides of 180° in the boreal winter of 2002: DSST increased to the west of 180° but decreased to the east (Fig. 5a). The corresponding time lag of DSST east of 180° was the same as that of wind speed (Fig. 5b), suggesting that the reversed wind speed anomalies were responsible for the reversed DSST anomalies in this region (Fig. 5a). A similar situation can also be observed in the boreal summer of 2002 (Figs. 5c and d).

Similar to the DSST responses, opposite responses to the MJO can be seen in latent heat flux anomalies on the two sides of 180° (150°E) in boreal winter (summer) (Figs. 4d and h). This is because intraseasonal latent heat flux anomalies are determined primarily by intraseasonal wind speed anomalies, which are of opposite signs. This suggests that opposite responses to the MJO be a common phenomenon for any variable that is closely related to wind speed. Indeed, this is confirmed by the opposite responses of evaporation rate or surface roughness to the MJO (Fig. 6).

## 4. Summary and discussion

In this study, the responses of DSST to the MJO in the tropical Indian and western central Pacific oceans, especially the responses of DSST to the reversed wind speed anomalies in the central tropical Pacific Ocean, are investigated using both the TAO/TRITON buoy data and an empirical model. The results show that the responses of DSST to the MJO are opposite for the tropical regions on the two sides of 180° (150°E) in boreal winter (summer): DSST decreases when the active convection center of the MJO is located to the west of 180° (150°E) but increases when the active convection center moves to the east of 180° (150°E) in boreal winter (summer). Further analysis demonstrates that the reversed wind speed anomalies east of 180° (150°E) in boreal winter (summer) are responsible for the reversed DSST anomalies in this region. This suggests that opposite responses to the MJO be a common feature for any variable that is closely related to wind speed.

Many studies have shown that the diurnal cycle of SST accounts for

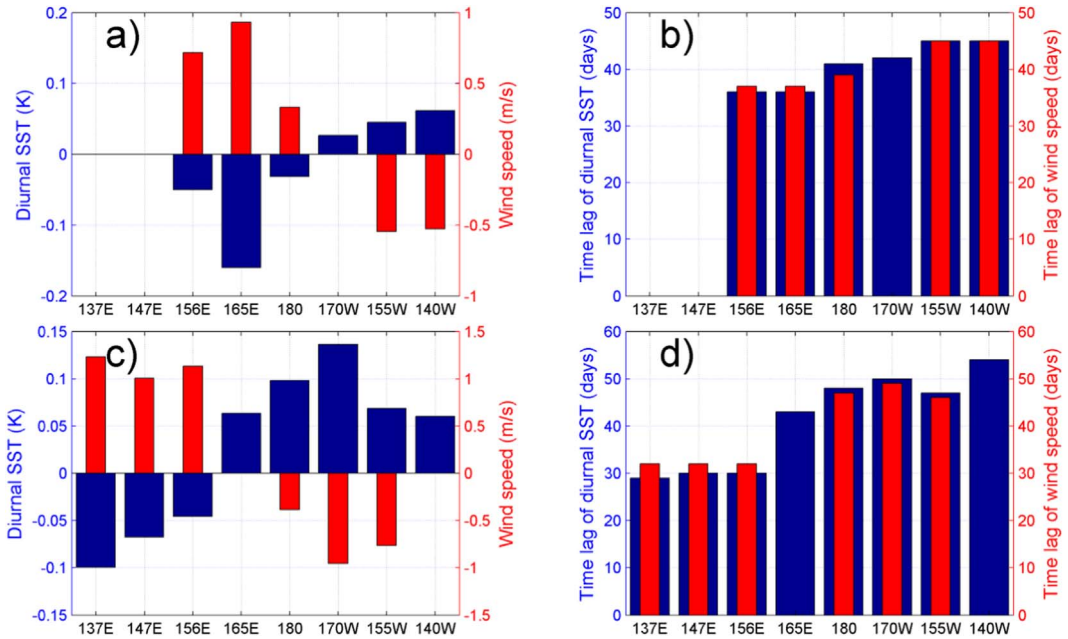


**Fig. 5.** The maximum amplitude of lagged regression of DSST (blue bars) and wind speed (red bars) on the MJO index RMM2 (large RMM2 appears in phases 6–7), and its corresponding time lag along 5°S during the boreal winter of 2002 (a, b), and along 5°N during the boreal summer of 2002 (c, d). To obtain scaled values, these regression coefficients are multiplied by one standard deviation of RMM2. Time lag is added by 36 (the MJO propagates from phase 1 to phases 6–7). DSST and wind speed are derived from the TAO/TRITON buoy data. Wind speeds at (170°W, 5°S) in the boreal winter of 2002 and at (165°E, 5°N) and (140°W, 5°N) in the boreal summer of 2002 are missing. (For interpretation of the references to color in this figure legend, the reader is referred to the web version of this article.)

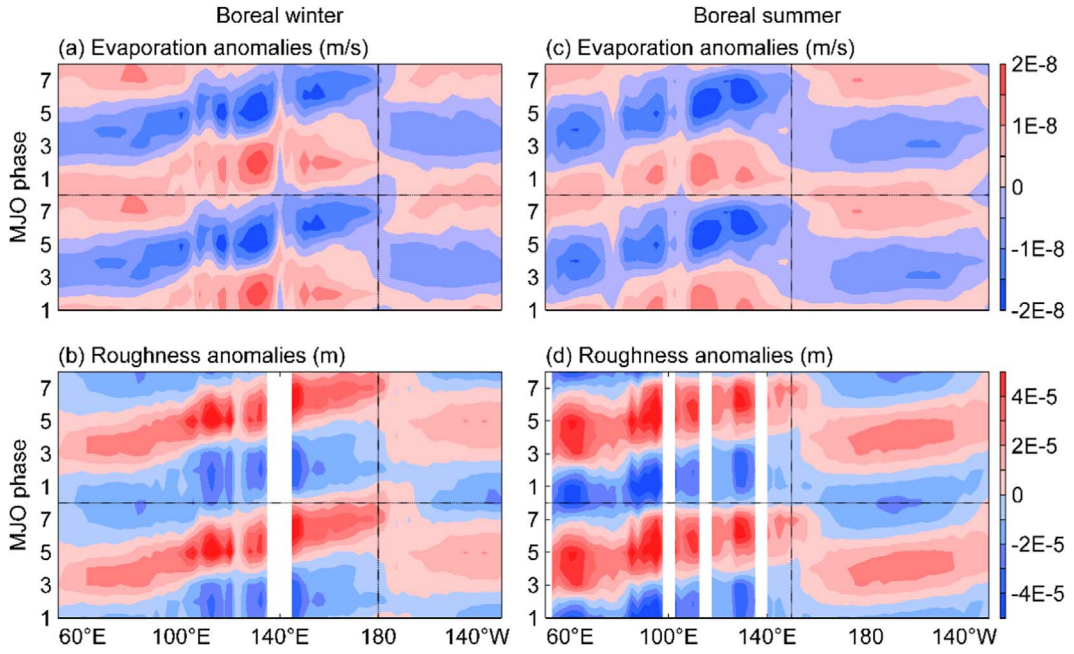


**Fig. 6.** Same as Fig. 4, except for (a, c) evaporation rate anomalies (positive downward, m/s) and (b, d) surface roughness anomalies (m) derived from the ERA-Interim global atmospheric reanalysis.

about 20–40% of the amplitude of the intraseasonal SST variability in the equatorial Indian and western tropical Pacific oceans (e.g., Bernie et al., 2005, 2007; Mujumdar et al., 2011). This is because larger DSST occurs during warming phase, increasing daily mean SST and enhancing the intraseasonal SST variability. In the central tropical Pacific Ocean, however, larger DSST does not occur during warming phase. The effect of the diurnal cycle of SST on the intraseasonal SST variability must be different there, which needs to be studied in the future.

## Acknowledgments

This study is supported by the National Natural Science Foundation of China (Grants 91428206, 41606017, 41621064, and 91528304), the National Key Research and Development Program of China (2016YFC1401601). The authors wish to express their appreciation to Dr. Zuojun Yu for English modification.

## References

Araligidad, N.M., Maloney, E.D., 2008. Wind-driven latent heat flux and the intraseasonal oscillation. Geophys. Res. Lett. 35, L04815.
Bernie, D., Woolnough, S., Slingo, J., Guilyardi, E., 2005. Modeling diurnal and intraseasonal variability of the ocean mixed layer. J. Clim. 18, 1190–1202.
Bernie, D., Guilyardi, E., Madec, G., Slingo, J., Woolnough, S., 2007. Impact of resolving the diurnal cycle in an ocean-atmosphere GCM. Part 1: a diurnally forced OGCM. Clim. Dyn. 29, 575–590.
Bellenger, H., Duvel, J.P., 2009. An analysis of tropical ocean diurnal warm layers. J. Clim. 22, 3629–3646. http://dx.doi.org/10.1175/2008JCLI2598.1.
Dee, D.P., et al., 2011. The ERA-Interim reanalysis: configuration and performance of the data assimilation system. Q. J. Roy. Meteorol. Soc. 137, 553–597.
Gentemann, C.L., Donlon, C.J., Stuart-Menteth, A., Wentz, F.J., 2003. Diurnal signals in satellite sea surface temperature measurements. Geophys. Res. Lett. 30 (3), 1140. http://dx.doi.org/10.1029/2002GL016291.
Gentemann, C.L., Minnett, P.J., Le Borgne, P., Merchant, C.J., 2008. Multi-satellite measurements of large diurnal warming events. Geophys. Res. Lett. 35, L22602. http://dx.doi.org/10.1029/2008GL035730.
Grodsky, S.A., Bentamy, A., Carton, J.A., Carton, R.T., 2009. Intraseasonal latent heat flux based on satellite observations. J. Clim. 22, 4539–4556. http://dx.doi.org/10.1175/2009JCLI2901.1.
Guemas, V., Salas-Melia, D., Kageyama, M., Giordani, H., Voldoire, A., 2013. Impact of the ocean diurnal cycle on the North Atlantic mean sea surface temperatures in a regionally coupled model. Dyn. Atmos. Oceans 60, 28–45.
Hendon, H.H., Glick, J., 1997. Intraseasonal air-sea interaction in the tropical Indian and Pacific Oceans. J. Clim. 10 (4), 647–661.
Jin, D., Waliser, D.E., Jones, C., Murtugudde, R., 2013. Modulation of tropical ocean surface chlorophyll by the Madden-Julian oscillation. Clim. Dyn. 40, 39–58.
Kawai, Y., Wada, A., 2007. Diurnal sea surface temperature variation and its impact on the atmosphere and ocean: a review. J. Oceanogr. 63, 721–744.
Kawai, Y., Kawamura, H., 2002. Evaluation of the diurnal warming of sea surface temperature using satellite-derived marine meteorological data. J. Oceanogr. 58, 805–814.
Kawai, Y., Kawamura, H., 2003. Validation of daily amplitude of sea surface temperature evaluated with a parametric model using satellite data. J. Oceanogr. 59, 637–644.
Kawai, Y., Kawamura, H., 2005. Spatial and temporal variations of model-derived diurnal amplitude of sea surface temperature in the western Pacific Ocean. J. Geophys. Res. 110, C08012. http://dx.doi.org/10.1029/2004JC002652.
Kennedy, J.J., Brohan, P., Tett, S.F.B., 2007. A global climatology of the diurnal variations in sea-surface temperature and implications for MSU temperature trends. Geophys. Res. Lett. 34, L05712. http://dx.doi.org/10.1029/2006GL028920.
Li, Y., Han, W., Shinoda, T., Wang, C., Lien, R.C., Moum, J.N., Wang, J.W., 2013. Effects of the diurnal cycle in solar radiation on the tropical Indian Ocean mixed layer variability during wintertime Madden-Julian oscillations. J. Geophys. Res. Oceans 118, 4945–4964. http://dx.doi.org/10.1002/jgrc.20395.
Madden, R.A., Julian, P.R., 1971. Detection of a 40–50 day oscillation in the zonal wind in the tropical Pacific. J. Atmos. Sci. 28, 702–708.
Madden, R.A., Julian, P.R., 1972. Description of global scale circulation cells in the tropics with a 40–50 day period. J. Atmos. Sci. 29, 1109–1123.
Madden, R.A., Julian, P.R., 2005. Historical perspective. In: Lau, W.K.M., Waliser, D.E. (Eds.), Intraseasonal Variability in the Atmosphere-Ocean Climate System. Praxis, Chichester, U.K., pp. 1–18.
Matthews, A.J., 2000. Propagation mechanisms for the Madden-Julian oscillation. Q J. R. Meteorol. Soc. 126, 2637–2652.
Milliff, R.F., Madden, R.A., 1996. The existence and vertical structure of fast, eastward-moving disturbances in the equatorial troposphere. J. Atmos. Sci. 53 (4), 586–597.
Mujumdar, M., Salunke, K., Rao, S.A., Ravichandran, M., Goswami, B.N., 2011. Diurnal cycle induced amplification of sea surface temperature intraseasonal oscillations over the Bay of Bengal in summer monsoon season. IEEE Geosci. Remote Sens. Lett. 8 (2), 206–210.
Sobel, A.H., Kim, D., 2012. The MJO-Kelvin wave transition. Geophys. Res. Lett. 39, L20808. http://dx.doi.org/10.1029/2012GL053380.
Stuart-Menteth, A.C., Robinson, I.S., Challenor, P.G., 2003. A global study of diurnal warming using satellite-derived sea surface temperature. J. Geophys. Res. 108 (C5), 3155. http://dx.doi.org/10.1029/2002JC001534.
Webster, P.J., Clayson, C.A., Curry, J.A., 1996. Clouds, radiation, and the diurnal cycle of sea surface temperature in the tropical western Pacific. J. Clim. 9, 1712–1730.
Wheeler, M.C., Hendon, H.H., 2004. An all-season real-time multivariate MJO index: development of an index for monitoring and prediction. Mon. Weather Rev. 132, 1917–1932.
Woolnough, S.J., Slingo, J.M., Hoskins, B.J., 2000. The relationship between convection and sea surface temperature on intraseasonal timescales. J. Clim. 13, 2086–2104.
Yang, Y., Li, T., Li, K.P., Yu, W.D., Liu, Y.L., 2015. Modulation of Madden-Julian Oscillation on the diurnal cycle of SST in the tropical Indian Ocean—results from one dimensional mixed layer model. Haiyang Xuebao 37 (5), 34–43.
Zhang, C., 2005. Madden-Julian Oscillation. Rev. Geophys. 43, RG2003. http://dx.doi.org/10.1029/2004RG000158.
Zhang, C., Dong, M., 2004. Seasonality of the Madden-Julian oscillation. J. Clim. 17, 3169–3180.